Crustal structure in Ethiopia and Kenya from receiver function analysis: Implications for rift development in eastern Africa

Mulugeta T. Dugda,[1] Andrew A. Nyblade,[1] Jordi Julia,[2] Charles A. Langston,[3] Charles J. Ammon,[1] and Silas Simiyu[4]

Received 5 March 2004; revised 29 September 2004; accepted 14 October 2004; published 6 January 2005.

[1] Crustal structure in Kenya and Ethiopia has been investigated using receiver function analysis of broadband seismic data to determine the extent to which the Cenozoic rifting and magmatism has modified the thickness and composition of the Proterozoic crust in which the East African rift system developed. Data for this study come from broadband seismic experiments conducted in Ethiopia between 2000 and 2002 and in Kenya between 2001 and 2002. Two methods have been used to analyze the receiver functions, the H-κ method, and direct stacks of the waveforms, yielding consistent results. Crustal thickness to the east of the Kenya rift varies between 39 and 42 km, and Poisson's ratios for the crust vary between 0.24 and 0.27. To the west of the Kenya rift, Moho depths vary between 37 and 38 km, and Poisson's ratios vary between 0.24 and 0.27. These findings support previous studies showing that crust away from the Kenya rift has not been modified extensively by Cenozoic rifting and magmatism. Beneath the Ethiopian Plateau on either side of the Main Ethiopian Rift, crustal thickness ranges from 33 to 44 km, and Poisson's ratios vary from 0.23 to 0.28. Within the Main Ethiopian Rift, Moho depths vary from 27 to 38 km, and Poisson's ratios range from 0.27 to 0.35. A crustal thickness of 25 km and a Poisson's ratio of 0.36 were obtained for a single station in the Afar Depression. These results indicate that the crust beneath the Ethiopian Plateau has not been modified significantly by the Cenozoic rifting and magmatism, even though up to a few kilometers of flood basalts have been added, and that the crust beneath the rifted regions in Ethiopia has been thinned in many places and extensively modified by the addition of mafic rock. The latter finding is consistent with models for rift evolution, suggesting that magmatic segments with the Main Ethiopian Rift, characterized by dike intrusion and Quaternary volcanism, act now as the locus of extension rather than the rift border faults.

Citation: Dugda, M. T., A. A. Nyblade, J. Julia, C. A. Langston, C. J. Ammon, and S. Simiyu (2005), Crustal structure in Ethiopia and Kenya from receiver function analysis: Implications for rift development in eastern Africa, *J. Geophys. Res.*, *110*, B01303, doi:10.1029/2004JB003065.

1. Introduction

[2] In this study, crustal structure has been investigated within and surrounding the eastern branch of the East African rift system in Ethiopia and Kenya to determine the extent to which crustal structure has been modified by the Cenozoic rifting and magmatism found there. The East African rift system is one of the largest continental rift systems on Earth, extending from the Afar region of Ethiopia southward to beyond the Zambezi River. Knowledge about the crustal structure of this rift system is important for not only improving our understanding of rifting mechanisms, but also for constraining models of rift-related plateau uplift and volcanism.

[3] Crustal structure has been determined from receiver function analysis of broadband seismic data recorded by temporary deployments of seismic stations in Ethiopia and Kenya. Our results provide new, first-order estimates of crustal thickness and Poisson's ratio beneath the Afar Depression, the Main Ethiopian Rift (MER), the Ethiopian Plateau, the Kenya Rift, and parts of the East African Plateau in Kenya, and when combined with previous results from Tanzania and Kenya, they can be used to examine the extent to which the crust has been modified within and surrounding the eastern branch of the East African rift system.

[1]Department of Geosciences, Pennsylvania State University, University Park, Pennsylvania, USA.
[2]Division of Earth and Ocean Sciences, Duke University, Durham, North Carolina, USA.
[3]Center for Earthquake Research and Information, University of Memphis, Memphis, Tennessee, USA.
[4]Kenya Power Generating Company, Naivasha, Kenya.

0148-0227/05/2004JB003065$09.00

[4] This paper is organized in several sections. In section 2, background information on the geology of eastern Africa is reviewed together with previous crustal structure studies and the 2000–2002 broadband seismic experiments in Ethiopia and Kenya. In section 3, receiver function modeling methods and data are discussed and results are presented. In section 4, using our results and those from previous studies, we comment on the nature of crustal modification associated with the eastern branch of the rift system.

2. Background Information

2.1. Geology

[5] The East African rift system has two branches, a western and an eastern branch (Figure 1). The main sectors of the eastern branch, from north to south, are the Main Ethiopian Rift, the Kenya (Gregory) Rift, and a wide (>300 km) region of block faulting in northern Tanzania. The Afar Depression is located at the northern end of the eastern branch. The tectonic development of the eastern branch, as well as the western branch, has been strongly controlled by Precambrian crustal evolution [*Nyblade and Brazier*, 2002]. The Archean Tanzania (Nyanza) Craton forms the nucleus of the Precambrian framework of eastern Africa and is surrounded by several Proterozoic mobile belts [*Cahen et al.*, 1984]. The Mozambique Belt, within which the eastern branch has developed, extends from Ethiopia south through Kenya, Tanzania and Mozambique and is located to the east of the craton. The Mozambique Belt is believed to represent a Himalayan-type continental collision zone [*Burke and Sengor*, 1986; *Shackleton*, 1986], and numerous sutures marked by dismembered ophiolites have been recognized within the basement complex of Ethiopia [e.g., *Berhe*, 1990; *Vail*, 1988, 1985]. The foreland to this collisional event in the south is the Tanzania Craton, and to the north it is in western Ethiopia under Cenozoic volcanic rocks [*Kroner et al.*, 1987].

[6] Rift evolution within the eastern branch is complicated and possibly developed separately in two regions. Volcanism began about 45–40 Ma in southwestern Ethiopia [*Davidson and Rex*, 1980; *Zanettin et al.*, 1980; *Berhe et al.*, 1987; *WoldeGabriel et al.*, 1990; *Ebinger et al.*, 1993; *George et al.*, 1998] and propagated to the south through Kenya and into northern Tanzania. In the northern part of the Kenya rift magmatic activity began in the Oligocene (circa 30 Ma) [*Morley et al.*, 1992; *Ritter and Kaspar*, 1997]. It commenced around 15 Ma in the central portion of the Kenya rift, at circa 12 Ma in southern Kenya [*Morley et al.*, 1992; *Hendrie et al.*, 1994; *Mechie et al.*, 1997], and at about 8 Ma in northern Tanzania [*Dawson*, 1992; *Foster et al.*, 1997; *Ebinger*, 1989]. The earliest Cenozoic rifting occurred circa 25 Ma in northern Kenya [*Morley et al.*, 1992; *Hendrie et al.*, 1994], and propagated southward reaching central Tanzania by circa 1 Ma [*Baker*, 1986; *Foster et al.*, 1997].

[7] In the future sites of the Red Sea, easternmost Gulf of Aden, and the central Ethiopian plateau, widespread volcanic activity initiated during the Oligocene (circa 29–31 Ma) with the emplacement of thick (500–2000 m) flood basalts and rhyolites within 1–2 Myr [*Hofmann et al.*, 1997; *Mohr and Zanettin*, 1988; *Mohr*, 1983; *Berhe et al.*, 1987; *Baker et al.*, 1996; *Ayalew et al.*, 2002; *Coulie et al.*, 2003]. Sitting on top of the flood basalts are less voluminous synrift shield volcanoes that formed between 30 and 10 Ma, locally creating an additional 1000 to 2000 m of relief [*Berhe et al.*, 1987; *Coulie et al.*, 2003]. Uplift of the Ethiopian Plateau commenced between 20 and 30 Ma, soon after the major flood basalts erupted [*Pik et al.*, 2003]. In contrast, timing of plateau uplift to the south in east Africa remains poorly constrained, although there is some evidence for Neogene rift flank uplift [*Noble et al.*, 1997; *van der Beek et al.*, 1997].

[8] The formation of the Red Sea and Gulf of Aden rifts began in the Oligocene when Africa began separating from Arabia and can be linked to the complex geometry of collision along the Alpine-Himalayan chain [*Bellahsen et al.*, 2003]. The opening of the eastern branch to form the Afar triple junction occurred long after the flood basalts erupted and Arabia separated from Africa. Extension commenced after 11 Ma in the central and northernmost sector of the MER [*Wolfenden et al.*, 2004; *Chernet et al.*, 1998; *WoldeGabriel et al.*, 1999] and at circa 18 Ma in southwestern Ethiopia [*Ebinger et al.*, 2000]. *Wolfenden et al.* [2004] suggest that there was a hiatus in volcanism between 6.5 and 3.2 Ma within the MER, after which time deformation migrated toward a narrow zone in the rift center, and that by 1.8 Ma volcanism and faulting had localized to magmatic segments within the rift. Most of the Quaternary volcanism in the MER has occurred within the magmatic segments, but it has also occurred along the rift shoulder in a number of places. Historical flows at Fantale [*Gibson*, 1967] and elevated temperatures at shallow crustal depths in the geothermal field near Aluto suggest that magmatic processes within the MER have been recently active. *Ebinger and Casey* [2001] proposed that the magmatic segments act now as the locus of extension within this transitional rift setting rather than the rift border faults.

[9] The volcanism, plateau uplift and rifting in eastern Africa cannot be explained easily by simple passive rifting related to the development of the Afar triple junction, and consequently many authors have invoked one or more mantle plumes to account for the Cenozoic tectonism. The multistage scenario of rift development described above can be attributed to multiple plumes (i.e., one at circa 45 Ma in southern Ethiopia and one at circa 30 Ma in the Afar region), however, others [e.g., *Manighetti et al.*, 1997; *Courtillot et al.*, 1999] have attributed the Cenozoic tectonism to a single plume at circa 30 Ma and continued rifting and magmatism since then. While our results do not directly shed new light on the nature of the plume activity, the information on crustal structure presented below provides important constraints on rift development and the extent to which the rifting and magmatism has altered the preexisting crust.

2.2. Results of Previous Crustal Structure Studies in the Region

[10] Using seismic refraction, surface wave dispersion, gravity and other geophysical data, crustal structure has been investigated in many parts of eastern Africa. Figure 2 summarizes Moho depths (H) and crustal Poisson's ratios (σ) reported in previous studies.

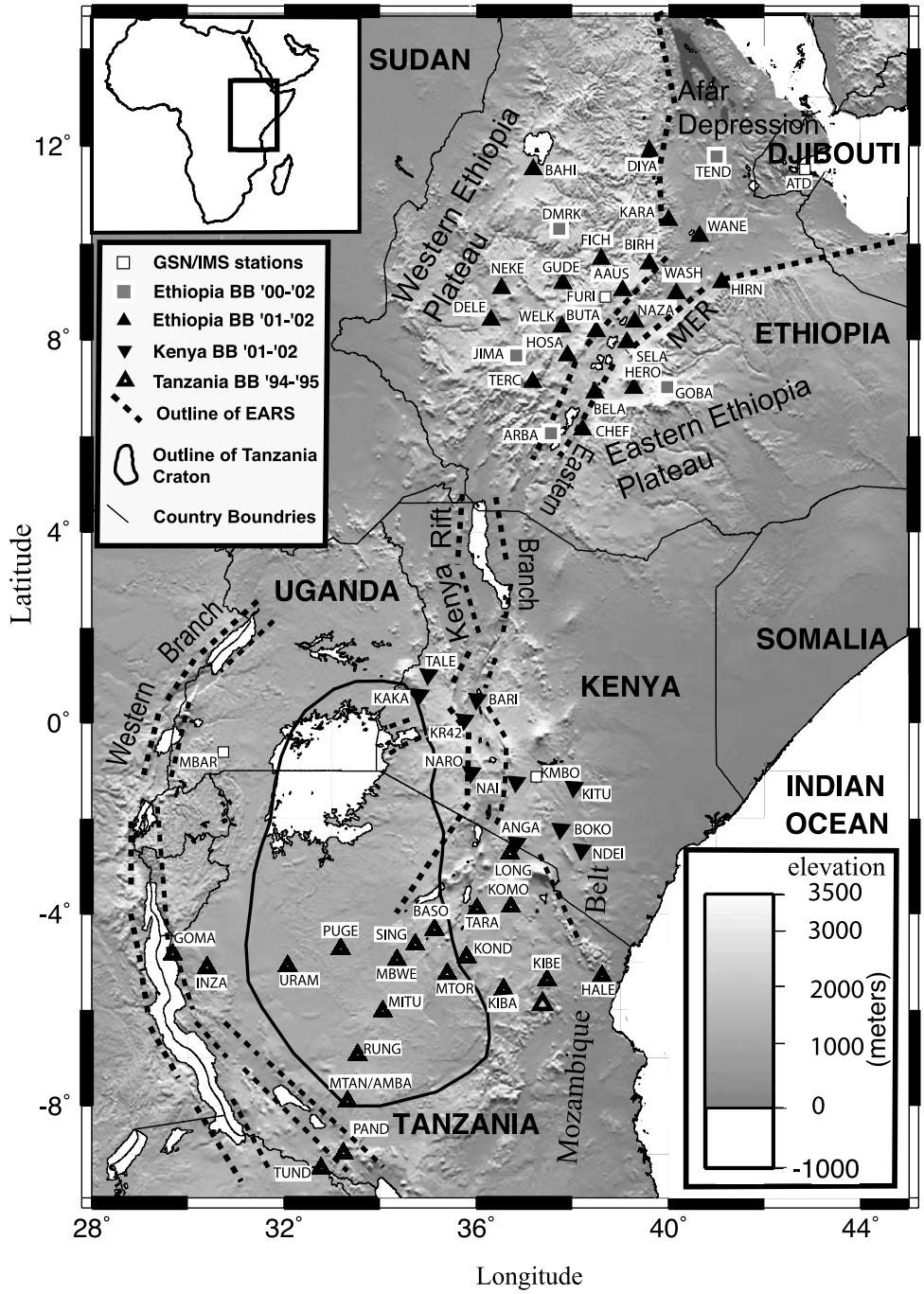

Figure 1. Location map of the study region showing topography, Precambrian terrains, the outline of the Cenozoic East African rift system, and the distribution of broadband seismic stations in Ethiopia, Kenya, and Tanzania.

[11] Using earthquake data, *Ruegg* [1975] and *Searle* [1975] estimated Poisson's ratio for the crust in Afar. *Searle* [1975] reported, from an analysis of surface waves crossing Afar, that Poisson's ratio increases from 0.25 at the surface to 0.27 to 0.29 at the deepest portion of the crust. On the other hand, *Ruegg* [1975] noted from deep seismic sounding studies in eastern Afar that Poisson's ratios as high as 0.33 characterize the region. *Searle and Gouin* [1971], from surface waves and body wave travel time data, placed an upper limit on the Moho depth beneath AAE (same location as AAUS, Addis Ababa, Figure 1) of 48 km. Using receiver functions, *Hebert and Langston* [1985] estimated a Moho depth of 41 km beneath AAE.

[12] The most detailed information about crustal structure in Ethiopia comes from seismic refraction surveys (lines I–VI, Figure 2) conducted in the mid-1970s [*Berckhemer et al.*, 1975]. *Makris and Ginzburg* [1987], revising the previous interpretation of *Berckhemer et al.* [1975], reported Moho depths of 33 to 44 km along profile I from west to

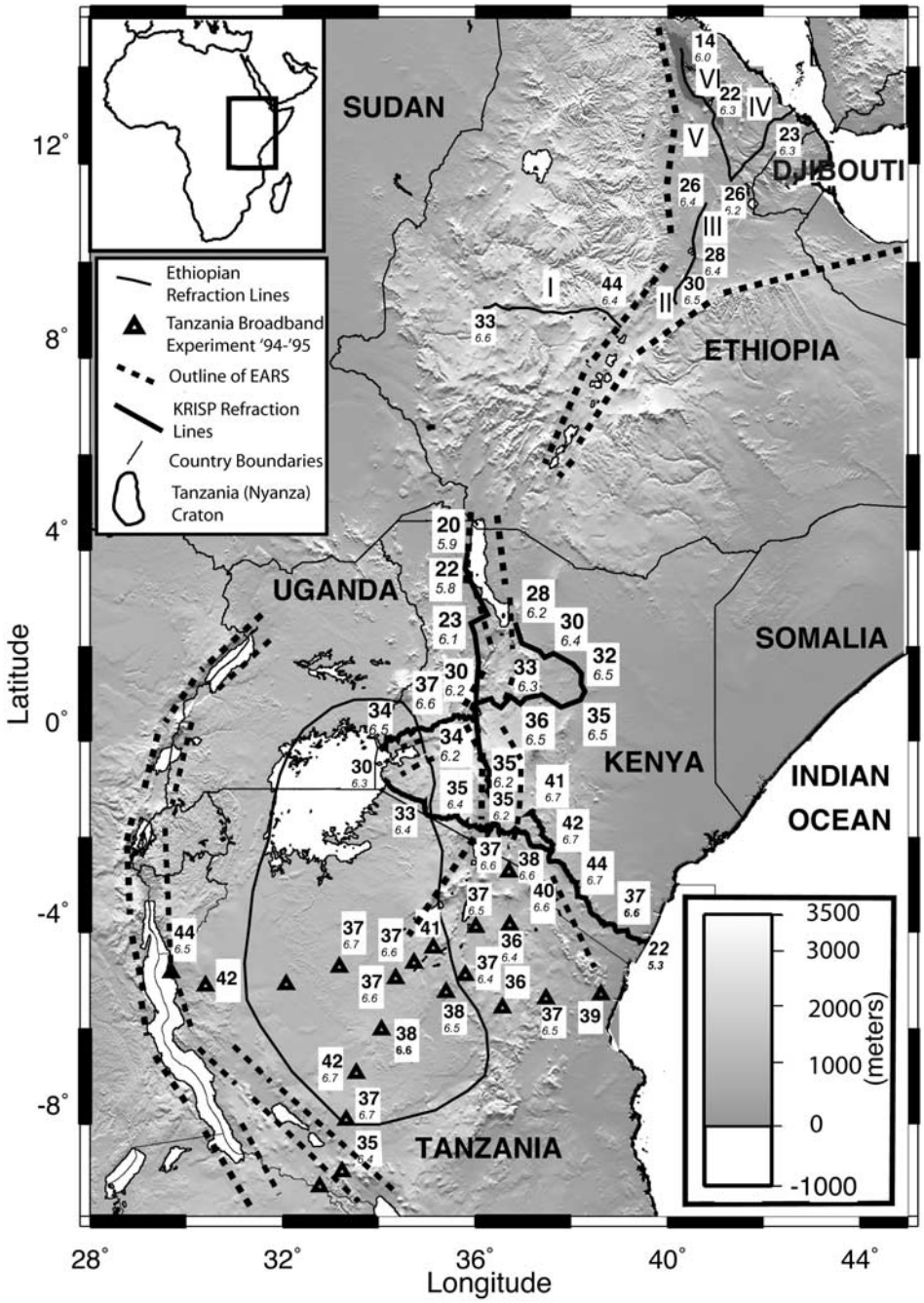

Figure 2. Map showing topography, Moho depths (in km), and average crustal *P* wave velocity estimates (in km/s) from eastern Africa. Moho depths are given in bold, while average crustal *P* wave velocities are indicated in italics. The average *P* wave velocities for the crust in Kenya and Ethiopia were determined from previous refraction studies. For Tanzania, they are from receiver functions. The geologic features are the same as in Figure 1.

east. Along refraction line II, they found a Moho depth of 30 km in the south and 26 km in the north, and for profiles V and VI, they found crustal thickness variations of 26 to 14 km, with a change in the middle of profile VI from about 26 km to about 20 km. For refraction line IV, they reported that crustal thickness thins from 26 to 23 km toward the Red Sea coast.

[13] Crustal structure in Kenya has been investigated by the Kenya Rift International Seismic Project (KRISP) project using refraction surveys [*Prodehl et al.*, 1994; *Fuchs et al.*, 1997, references therein]. As illustrated in Figure 2, crustal thickness in Kenya along the rift axis varies from 20 km in the north to 35 km in the south, and the average *P* wave velocity varies from 5.8 km/s to 6.2 km/s. To the west of the rift, Moho depth varies from 30 to 37 km while average *P* wave velocity varies from 6.2 to 6.6 km/s. To the east of the rift, the crustal thickness changes from 20 km near the coast to 44 km just north of Mt. Kilimanjaro and

Table 1. Teleseismic Events Used for Computing Receiver Functions

Date (Julian)	Time, UT	Latitude, deg	Longitude, deg	Depth, km	Distance, deg	Back Azimuth, deg
098, 2000	19.08	−18.045	65.517	10	39.8	135.6
133, 2000	23.1	35.975	70.657	108	39.7	44.1
157, 2000	3	−5.605	102.886	33	67.6	100.6
158, 2000	9.58	−5.093	102.699	33	67.3	100.2
159, 2000	23.45	−4.612	101.905	33	66.4	99.8
161, 2000	8	−5.549	102.679	33	67.4	100.6
190, 2000	4.52	−5.408	102.7	33	67.4	100.5
199, 2000	22.53	36.283	70.924	141	40.1	43.9
207, 2000	14.29	−53.553	−3.169	10	73.3	204.2
214, 2000	18.54	−38.765	78.419	10	62.5	144.7
235, 2000	16.55	38.117	57.376	10	33.2	29.3
245, 2000	11.56	1.438	96.591	33	59.8	94.5
252, 2000	1.34	−39.841	41.762	10	50.6	176.0
256, 2000	0.27	35.389	99.343	10	61.7	55.3
266, 2000	18.22	−4.964	102.104	33	66.7	100.2
267, 2000	2.17	4.276	−32.607	10	70.7	270.8
269, 2000	4	−46.806	37.59	10	57.5	180.1
279, 2000	13.39	31.732	−40.958	10	75.9	300.2
281, 2000	11.57	−9.974	119.378	33	84.7	101.3
295, 2000	11.35	−47.347	−12.403	10	73.4	213.2
299, 2000	9.32	−6.549	105.63	38	70.5	100.9
304, 2000	12.01	−9.708	119.075	33	84.3	101.1
312, 2000	0.18	−55.627	−29.876	10	87.2	211.7
330, 2000	18.09	40.245	49.946	50	32.1	17.9
341, 2000	17.11	39.566	54.799	30	33.2	24.7
350, 2000	16.44	38.457	31.351	10	28.9	349.5
015, 2001	5.52	−40.344	78.362	10	63.6	146.0
045, 2001	4.45	−5.164	102.488	33	67.1	100.3
049, 2001	13.04	−47.456	32.386	10	58.4	184.3
052, 2001	15.22	−4.9	102.45	33	67.0	100.0
054, 2001	0.09	29.513	101.129	33	62.6	62.1
016, 2001	13.25	−4.022	101.776	28	66.7	93.9
026, 2001	3.16	23.419	70.232	16	41.8	51.7
028, 2001	1.02	23.507	70.517	10	42.1	51.8
044, 2001	19.28	−4.68	102.562	36	67.5	94.6
047, 2001	5.59	−7.161	117.488	520	82.5	97.0
055, 2001	7.23	1.271	126.249	35	91.5	88.7
055, 2001	16.33	1.555	126.431	33	91.7	88.5
056, 2001	2.21	36.424	70.881	202	50.1	37.5
064, 2001	15.5	34.369	86.902	33	60.0	48.4
066, 2001	18.1	−6.81	−12.911	10	49.6	262
073, 2001	18.56	45.1	121.892	109	87.1	89.5
074, 2001	1.22	8.656	94.013	33	59.4	79.2
078, 2001	5.52	−4.029	128.02	33	93.2	94.0
103, 2001	15.33	−59.723	−25.586	26	75.9	207.4
207, 2001	0.21	39.059	24.244	10	41.8	346.3
217, 2001	5.16	12.224	93.352	96	59.3	75.1
239, 2001	1.16	1.091	126.36	33	89.4	88.9
250, 2001	2.45	−13.166	97.297	10	60.5	104.4
287, 2001	1.1	−8.598	110.633	67	73.5	98.5
318, 2001	9.26	35.946	90.541	10	62.1	47.2
327, 2001	20.43	36.392	71.506	106	49.4	36.3
339, 2001	7.46	−52.606	18.349	10	54.2	194.8
347, 2001	13.5	27.042	−44.496	10	84.9	297.2
352, 2001	4.02	23.954	122.734	14	86.7	66.0

the average *P* wave velocity varies from 6.2 to 6.7 km/s. To the east of the central Kenya rift the crustal thickness varies between 35 and 36 km while the average *P* wave velocity is about 6.5 km/s.

[14] In Tanzania, crustal structure has been studied by *Last et al.* [1997] using a combination of receiver functions and Rayleigh wave dispersion measurements (Figure 2). *Last et al.* [1997] found Moho depths of 37 to 42 km for the Tanzania Craton, 36 to 39 km for the Mozambique Belt, and 40 to 45 km for the Ubendian Belt. Poisson's ratios vary between 0.24 and 0.26 for the Tanzania Craton, between 0.24 and 0.27 for the Mozambique Belt, and between 0.24 and 0.25 for the Ubendian Belt [*Last et al.*, 1997].

2.3. Ethiopia and Kenya Broadband Seismic Experiments

[15] Seismic data collected between 2000 and 2002 by the Ethiopia and Kenya Broadband Seismic Experiments are used in this study together with data from permanent stations in the region (Figure 1). Detailed information on the station configuration, recording parameters, and other related information is reported by *Nyblade and Langston*

[2002]. In Ethiopia, 22 of the 27 stations were located either on the eastern or western side of the Ethiopian Plateau (Figure 1). The rest of the stations in Ethiopia were situated in the Main Ethiopian Rift or Afar Depression. In Kenya, 1 station was located within the rift, 5 to the west and 4 to the east of the rift.

3. Crustal Structure of the Study Area From Receiver Functions

3.1. Methods and Data

[16] Receiver function analysis has been used to examine crustal structure for many years [e.g., *Langston*, 1979]. In this study, "simple stacks" of receiver functions and the H-κ stacking technique (H = Moho depth and $\kappa = V_p/V_s$) [*Zhu and Kanamori*, 2000] are used to estimate the thickness and Poisson's ratio of the crust. "Simple stack" refers to the common stacking method, in which the receiver function traces obtained from a station are averaged. The *Ps* and *PpPs* phase arrival times are then used to determine Moho depth and Poisson's ratio (or V_p-to-V_s ratio) following the equations derived by *Zandt et al.* [1995].

[17] It is well known that H and the κ trade off strongly [*Ammon et al.*, 1990; *Zandt et al.*, 1995]. In an effort to reduce the ambiguity introduced by this trade-off, *Zhu and Kanamori* [2000] incorporated the later arriving crustal reverberations *PpPs* and *PpSs + PsPs* in a stacking procedure whereby the stacking itself transforms the time domain receiver functions directly to objective function values in H-κ parameter space. The objective function for the stacking is

$$s(H,\kappa) = \sum_{j=1}^{N} w_1 r_j(t_1) + w_2 r_j(t_2) - w_3 r_j(t_3) \qquad (1)$$

where w_1, w_2, w_3 are weights, $r_j(t_i)$, i = 1, 2, 3, are the receiver function amplitude values at the predicted arrival times of the *Ps*, *PpPs*, and *PsPs + PpSs* phases, respectively, for the jth receiver function, and N is the number of receiver functions used. The stacked receiver function should attain its maximum value when H and κ are correct. By performing a grid search through H and κ parameter space, the H and κ values corresponding to the maximum value of the objective function can be determined [*Zhu and Kanamori*, 2000].

[18] The H-κ method provides a better estimate of Moho depth and V_p/V_s ratio than the "simiple stack" method because it uses the correct ray parameter for stacking each event. We use both methods in this study because previous results from Tanzania used the "simple stack" method [*Last et al.*, 1997], and therefore to assess the robustness of any comparison between our best estimates using H-κ stacking and those published for Tanzania, we need to check for systematic differences that might arise from employing the two methods.

[19] Table 1 summarizes important event information. Events come from distances of 30°–100° and have magnitudes greater than 5.5. Most of the events are from the north (Hindu Kush–Pamir region) or the east (the Indonesian and western Pacific subduction zones). For computing the receiver functions, a time domain iterative deconvolution method [*Ligorria and Ammon*, 1999] was used, and to evaluate the quality of the receiver functions, a least squares misfit criterion was applied. The misfit criterion provides a measure of the closeness of the receiver functions to an ideal case, and it is calculated by using the difference between the radial component and the convolution of the vertical component with the already determined radial receiver function. Usually receiver functions with a fit of 90% and above are used in our analysis. However, in a few cases, when it was difficult to get a reasonable number of receiver functions for a station, receiver functions with fits of 70–90% were included. Figures showing the receiver functions used for each station are given by *Dugda* [2003].

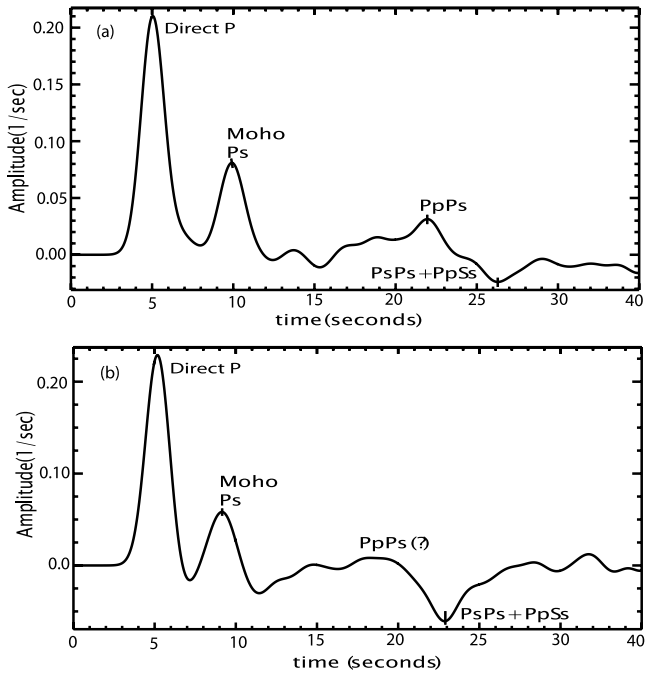

Figure 3. Examples of simple stacks of receiver functions. (a) An example of a simple stack of receiver functions from station HIRN showing clear *Ps*, *PpPs*, and *PsPs + PpSs* arrivals. (b) Simple stack of receiver functions from station CHEF showing clear *Ps* and *PsPs + PpSs* arrivals.

[20] The receiver functions were filtered with a Gaussian pulse width of 1.0. Both radial and tangential receiver functions were examined for evidence of lateral heterogeneity in the crust and for dipping structure. Events with large amplitude tangential receiver functions were not used. Stations identified with complicated structure are treated separately in section 3.4.

3.2. Crustal Models From Simple Stacks

[21] As mentioned earlier, the first approach applied in this study makes use of a simple stack of receiver functions and the arrival times of the *Ps* and *PpPs* phases. An example of a simple receiver function stack is given in Figure 3. For most stations, the *Ps* and *PpPs* phases were easily picked on the receiver functions, but the *PsPs + PpSs* phase was not (Figure 3a). However, for receiver functions at one station, the *PsPs + PpSs* phase was more clearly identifiable than the *PpPs* phase, and in that case the later arriving phase was picked for the computation of H and

Table 2. Results of Simple Stacks of Receiver Functions for a Plausible Range of Mean Crustal *P* Wave Velocities

	Phases Picked			V_p = 6.3 km/s			V_p = 6.5 km/s			V_p = 6.8 km/s			
Station	*Ps*	*PpPs*	*PsPs + PpSs*	Moho Depth, km	Poisson's Ratio	V_s, km/s	Moho Depth, km	Poisson's Ratio	V_s, km/s	Moho Depth, km	Poisson's Ratio	V_s, km/s	(Moho_Depth)/V_p, s
							Ethiopia						
AAUS	x	x		35.9	0.31	3.32	37.2	0.31	3.44	39.3	0.30	3.62	5.74 ± 0.04
ARBA[a]	x	x		29.2	0.26	3.60	30.3	0.26	3.72	32.0	0.25	3.92	4.67 ± 0.04
BAHI	x	x		42.9	0.26	3.59	44.4	0.258	3.71	46.8	0.25	3.90	6.84 ± 0.04
BELA[a]	x	x		37.3	0.32	3.26	38.6	0.32	3.31	40.7	0.31	3.54	5.95 ± 0.04
BIRH	x	x		41.4	0.27	3.56	42.8	0.27	3.67	44.8	0.26	3.85	6.58 ± 0.01
BUTA[b]	x			28.0	0.31	3.31	28.8	0.31[b]	3.41	30.1	0.31	3.57	4.43 ± 0.01
CHEF[c]	x		x	31.7	0.27	3.52	32.9	0.27	3.64	34.5	0.27	3.82	5.05 ± 0.02
DELE	x	x		35.5	0.27	3.55	36.8	0.26	3.68	38.8	0.26	3.87	5.67 ± 0.04
DIYA	x	x		35.9	0.24	3.7	37.2	0.23	3.83	39.2	0.23	4.02	5.73 ± 0.03
DMRK	x	x		38.8	0.26	3.56	40.2	0.26	3.69	42.4	0.26	3.87	6.20 ± 0.04
FICH[b]	x			32.7	0.28	3.48	33.7	0.28	3.59	35.1	0.28	3.76	5.17 ± 0.02
FURI	x	x		42.1	0.23	3.73	43.7	0.23	3.86	46.1	0.22	4.06	6.73 ± 0.05
GOBA	x	x		42.2	0.23	3.73	43.7	0.23	3.86	46.0	0.22	4.05	6.73 ± 0.03
GUDE	x	x		37.9	0.23	3.72	39.3	0.23	3.85	41.3	0.23	4.04	6.04 ± 0.03
HERO	x	x		40.7	0.26	3.6	42.2	0.26	3.72	44.4	0.25	3.91	6.50 ± 0.04
HIRN	x	x		40	0.26	3.61	41.3	0.25	3.73	43.4	0.25	3.91	6.36 ± 0.02
HOSA (N)	x	x		36.5	0.28	3.46	38	0.28	3.59	40.3	0.28	3.79	5.86 ± 0.07
HOSA (E)	x	x		35.2	0.31	3.28	36.4	0.31	3.4	38.3	0.31	3.57	5.61 ± 0.02
JIMA	x	x		33.7	0.29	3.45	34.9	0.28	3.57	36.8	0.28	3.75	5.38 ± 0.03
KARA	x	x		44.9	0.27	3.55	46.5	0.26	3.67	48.9	0.26	3.86	7.16 ± 0.03
NAZA[a]	x	x		26.5	0.35	3.06	27.4	0.34	3.17	29.0	0.34	3.34	4.24 ± 0.03
NEKE	x	x		32.2	0.28	3.5	33.4	0.27	3.62	35.2	0.27	3.81	5.15 ± 0.04
SELA[a] (N)	x	x		27.8	0.34	3.1	28.9	0.34	3.21	30.7	0.34	3.39	4.46 ± 0.05
TEND	x	x		23.2	0.33	3.17	24.1	0.33	3.28	25.4	0.33	3.45	3.71 ± 0.03
TERC	x	x		32.4	0.26	3.58	33.6	0.26	3.7	35.4	0.26	3.89	5.17 ± 0.04
WANE[a]	x	x		27.6	0.29	3.43	28.7	0.29	3.55	30.2	0.28	3.73	4.41 ± 0.03
WASH[a]	x	x		32.3	0.32	3.25	33.5	0.32	3.37	35.4	0.31	3.54	5.17 ± 0.04
WELK	x	x		31.5	0.28	3.5	32.6	0.28	3.62	34.3	0.27	3.8	5.02 ± 0.02
							Kenya						
ANGA	x	x		37.1	0.26	3.61	38.6	0.25	3.74	40.9	0.25	3.95	5.95 ± 0.06
BARI[d]	x			31.7	0.29	3.42	31.7	0.30	3.48	31.7	0.31	3.57	4.85 ± 0.2
BOKO[e]													
KAKA	x	x		37.1	0.23	3.75	38.4	0.22	3.88	40.5	0.22	4.08	5.93 ± 0.04
KITU[b]	x	x		37.1	0.26	3.59	38.2	0.26	3.70	39.8	0.26	3.87	5.87 ± 0.02
KMBO	x	x		40.0	0.26	3.58	41.5	0.26	3.70	43.6	0.26	3.89	6.38 ± 0.03
KR42	x	x		36.9	0.26	3.59	38.1	0.26	3.71	40.1	0.26	3.89	5.88 ± 0.02
NAI	x	x		41.0	0.26	3.61	42.5	0.26	3.73	44.7	0.25	3.92	6.54 ± 0.03
NARO[e]													
NDEI	x	x		38.7	0.25	3.64	40.0	0.25	3.76	42.1	0.24	3.95	6.17 ± 0.03
TALE	x	x		35.6	0.28	3.51	36.8	0.27	3.63	38.8	0.27	3.81	5.68 ± 0.03
							Uganda						
MBAR	x	x		31.2	0.30	3.36	32.3	0.30	3.47	34.1	0.30	3.65	4.98 ± 0.03

[a]Stations in the MER.
[b]Poisson's ratio assumed from nearby stations.
[c]*PsPs + PpSs* phase was picked instead of *PpPs* phase.
[d]Moho depth was taken from KRISP line to compute Poisson's ratio.
[e]Data too noisy to identify phases.

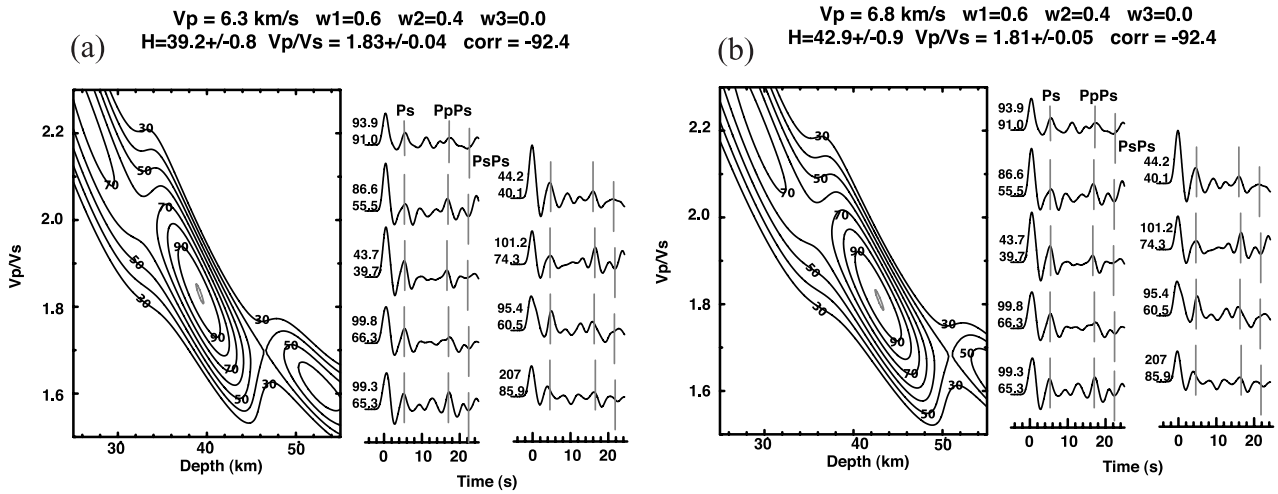

Figure 4. H-κ stacks of receiver functions for a range of V_p values for station DMRK. (a) V_p = 6.3 km/s and (b) V_p = 6.8 km/s. To the left of each receiver function, the top number gives the event azimuth, and the bottom number gives the event distance in degrees. Contours map out percentage values of the objective function given in the text.

Poisson's ratio (Figure 3b). For parameter determination, average ray parameters were used.

[22] Possible errors involved in picking the arrival times of the *Ps* and *PpPs* phases are about ±0.05 s. Computed H, V_s, and Poisson's ratios for a plausible range of values of V_p are given in Table 2. It is observed from the ratio of Moho depth estimates to the assumed V_p values that the P wave travel time in the crust is independent of the assumed value of V_p (Table 2).

3.3. Crustal Models From the H-κ Stacking Method

[23] In applying the H-κ technique, it is necessary to select weights w_1, w_2, and w_3, and a value for V_p. More weight is typically given to the phase that is most easily picked. As illustrated in Figure 4, given a range of plausible values for V_p (6.3 to 6.8 km/s), crustal thickness can vary by almost 4 km while the V_p/V_s ratio can change by 0.02. Thus, when estimating errors for the H-κ method, the uncertainty in mean crustal velocity, as well as the sensitivity of our results to variations in weights (w_1, w_2, w_3), must be considered.

[24] We use the H-κ stacking together with a perturbation analysis and a bootstrap algorithm to simultaneously find the best values of H and κ and the errors associated with these values. We begin by incorporating uncertainty in mean crustal velocity into error estimates for H and κ by specifying a normal distribution of V_p values so that 95% of the values selected fall between 6.2 and 6.8 km/s, with a mean value of 6.5 km/s. For the weights (w_1, w_2, w_3), we also use a normal distribution such that 95% of the values for w_1 fall between 0.55 and 0.65 with a mean of 0.6, for w_2 they fall between 0.25 and 0.35 with a mean value of 0.3, and for w_3 they vary between 0.05 and 0.15 with a mean value of 0.1.

[25] Once values for V_p and the weights are selected, we then use the bootstrap algorithm of *Efron and Tibshirani* [1991], together with the H-κ stacking, to estimate H and κ with statistical error bounds. While performing the H-κ stacking, the contribution of each of the receiver functions to the determination of H and κ is also weighted based on the least squares misfit value of the receiver functions. The procedure of selecting V_p and weights from the distribution described above and then performing the H-κ stacking with bootstrapping was repeated 200 times. After each time, new average values of H and κ and their uncertainties were computed. It was found that after repeating the procedure 50–60 times (out of 200), the error values for H and κ stabilized.

[26] Table 3 summarizes the results together with the error estimates obtained. The error estimates in H range from 1.2 km to 5.4 km and the average is 2.9 km. The error estimates for κ range from 0.03 to 0.18 and the average is 0.07.

3.4. Special Cases

[27] For some stations, receiver functions obtained using data from the two major source directions (north and east) give different results. For station SELA, events coming from the north sample the crust under the MER and give a Moho depth of ~27 km and Poisson's ratio of 0.34 (Figure 5). Events coming from the east sample the crust under the eastern plateau and MER, producing a complicated receiver function with no obvious *PpPs* or *PsPs* + *PpSs* phases. A Moho depth of 27 km and a Poisson's ratio of 0.34 are consistent with results from other stations in the MER (i.e., NAZA, WASH, and WANE). For HOSA, receiver functions from events sampling the crust to the north and east of the station yield similar Moho depth estimates of 37 km, but different Poisson's ratios; 0.28 for the crust beneath the western Ethiopia Plateau and 0.31 for the crust beneath the MER (Figure 5).

[28] For stations BUTA, KITU, and BARI (Figures 5 and 6) it was difficult to identify the *PpPs* and *PsPs* + *PpSs* phases, although the Moho *Ps* phase was clear. To estimate H for BUTA (Table 2), only events coming from the east that sample the crust beneath the MER were used together with the Poisson's ratio obtained for the nearby station HOSA (0.31) for the MER crust. The Moho *Ps* could not be easily identified for events coming from the north at BUTA. For station KITU, Poisson's ratio from the nearby station KMBO (0.26) was used to estimate Moho depth (Table 2).

Table 3. Results From H-κ Stacking of Receiver Functions

Station	Moho Depth, km	Depth Uncertainties	V_p/V_s	V_p/V_s Uncertainties	Poisson's Ratio σ	Number of Events
			Ethiopia			
AAUS	37	2.7	1.92	0.09	0.31	6
ARBA	30	2.6	1.80	0.18	0.27	12
BAHI	44	2.6	1.81	0.05	0.27	9
BELA	38	2.2	1.97	0.05	0.33	6
BIRH	41	3.6	1.84	0.09	0.28	5
BUTA[a]						
CHEF	37	5.37	1.72	0.14	0.28	5
DELE	36	4.16	1.83	0.13	0.28	4
DIYA	37	2.9	1.73	0.08	0.24	9
DMRK	41	2.4	1.83	0.05	0.28	9
FICH[a]						
FURI	44	4.5	1.74	0.09	0.26	9
GOBA	42	2.6	1.75	0.06	0.26	8
GUDE	41	4.3	1.66	0.10	0.22	5
HERO	42	2.2	1.83	0.03	0.28	10
HIRN	41	3.5	1.76	0.07	0.25	4
HOSA(E)	37	2.8	1.96	0.06	0.31	4
JIMA	36	1.2	1.85	0.06	0.29	10
KARA	44	4.5	1.85	0.12	0.27	8
NAZA	27	2.0	2.21	0.06	0.35	7
NEKE	34	2.4	1.81	0.06	0.27	10
SELA	27	1.6	2.26	0.07	0.34	7
TEND	25	1.5	2.16	0.05	0.36	11
TERC	34	2.4	1.78	0.05	0.26	17
WANE	30	1.9	1.92	0.08	0.32	7
WASH	35	3.5	1.91	0.08	0.32	12
WELK	33	2.4	1.83	0.07	0.27	11
			Kenya			
ANGA	39	3.0	1.7	0.07	0.24	6
BARI[b]						
BOKO[c]						
KAKA	37	2.0	1.67	0.07	0.24	3
KITU	40	3.9	1.73	0.07	0.25	9
KMBO	41	2.6	1.74	0.05	0.26	10
KR42	38	4.8	1.81	0.16	0.28	5
NAI	42	2.3	1.75	0.04	0.26	15
NARO[c]						
NDEI [d]						
TALE	38	3.2	1.76	0.04	0.27	4
			Uganda			
MBAR	33	3.3	1.88	0.13	0.3	7

[a]The ratio σ assumed from nearby stations because *PpP*s is not clear.
[b]Moho depth taken from KRISP refraction results to determine the σ value.
[c]Unable to identify Moho *Ps* phase.
[d]Too few high-quality data to use H-κ stacking.

For BARI, the Moho depth estimate from the KRISP refraction profile (Figure 2) was used, as the refraction line passed adjacent to this station. The Moho *Ps* was then used to determine the Poisson's ratio for the crust beneath this station (0.29, Table 2). For CHEF, the *PsPs* + *PpSs* phases were clear, but it was difficult to identify the *PpPs* reverberation (Figure 4b). Thus the Moho *Ps* and the *PpSs* + *PpSs* phases were used to estimate Moho depth and Poisson's ratio (Table 3). For NARO and BOKO, the data were too noisy to identify *Ps* phases, and therefore no results are reported for these stations.

[29] For many stations, the receiver functions show a trough in between the Moho *Ps* phase and the direct *P* wave arrival (stations BUTA, DMRK, FICH, FURI, HERO, KARA, NAZA, SELA, TEND, WANE, BARI, KR42, TALE; Figures 5 and 6). This is probably due to a shallow low-velocity zone near the surface created by high-velocity flood basalts overlying lower-velocity upper crustal sedimentary or felsic crystalline rock.

4. Discussion

[30] In this section we examine the extent to which the crust within and surrounding the eastern branch has been modified by the Cenozoic tectonism. As mentioned earlier, two approaches to analyzing the receiver functions were used to assess the robustness of a comparison between our results and those published for Tanzania by *Last et al.* [1997]. For our data set, the two approaches of analyzing receiver functions yield consistent results. In almost all cases, the differences in the results of the two approaches are within the error bounds of the estimates, and the differences between the Moho depth estimates are less than about 2 km (Tables 2 and 3). Therefore we conclude that our

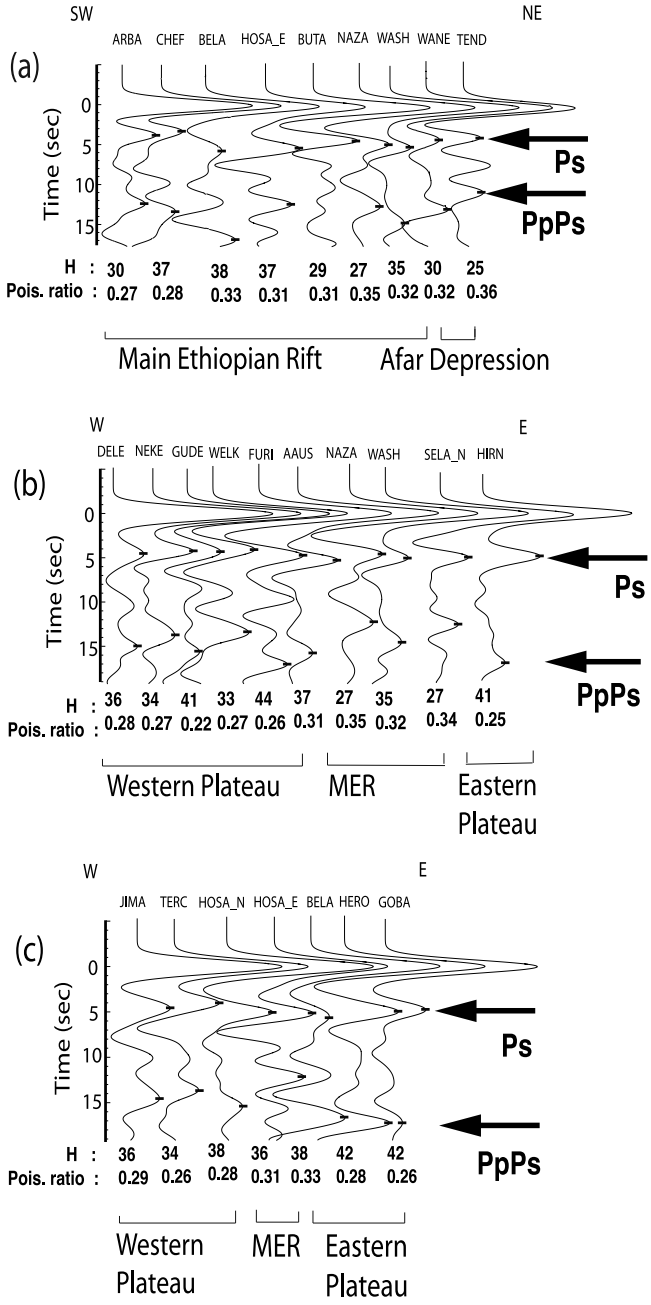

Figure 5. Profiles showing simple receiver function stacks for stations in Ethiopia. (a) SW-NE profile showing stations in the Main Ethiopian Rift and Afar. (b) W-E profile at ~9°N latitude. (c) W-E profile at ~7°N latitude. *H* and Poisson's ratio are from Table 3.

results from the *H*-κ stacking method can be compared directly to those from Tanzania without introducing any significant bias into our interpretation.

[31] For our examination of crustal structure, we use Poisson's ratio as a general indicator of bulk crustal composition. Below the melting point of many rocks, mineralogy is the most important factor influencing Poisson's ratio [*Christensen*, 1996], with the abundance of quartz and plagioclase feldspar having a dominant effect on common igneous rocks. For example, granitic rocks have a Poisson's ratio of about 0.24, while intermediate composition rocks (e.g., diorite) have values of around 0.27, and mafic rocks (e.g., gabbro) about 0.30 [*Christensen*, 1996; *Tarkov and Vavakin*, 1982]. Poisson's ratios as high as 0.32 have been reported for oceanic crust [*Bratt and Solomon*, 1984] and reflect the major crustal lithologies of basalt, diabase and gabbro. However, in continental settings, a Poisson's ratio above 0.30 (except for serpentinite) is rare and often indicates the presence of partial melt [*Watanabe*, 1993; *Owens and Zandt*, 1997].

[32] Profiles of receiver function stacks, Moho depth (*H*), and Poisson's ratio (σ) are illustrated in Figures 5 and 6, and Figure 7 shows a map of *H* and σ values for all the stations in eastern Africa. Table 4 summarizes average crustal structure for Precambrian crust along with the results obtained here and is provided for comparison purposes.

[33] We begin by discussing crustal structure in Kenya and Tanzania, focusing on areas of the crust away from the main rift valleys. Our estimates of crustal structure in Kenya are in good agreement with previous studies. *Hebert and Langston* [1985] estimated a crustal thickness of 41 ± 3 km beneath Nairobi, similar to the 42 km thick crust beneath Nairobi obtained in this study. To the west of the Kenya rift, crustal thickness of 37 and 38 km were found for KAKA and TALE, respectively (Figure 7), close to the 37 km crust obtained near the middle of the KRISP refraction line running from the Kenya rift to Lake Victoria (Figure 2). To the east of the Kenya rift, crustal thickness is in the range of 39 to 42 km, which is very close to the range of values reported on the KRISP refraction lines (Figure 2). Poisson's ratios for the crust to the east and west of the Kenya rift range from 0.24 to 0.27.

[34] When these estimates for Moho depth and Poisson's ratio are compared to estimates from stations in the Mozambique Belt in Tanzania (Figure 7), as well as to global average values for Proterozoic crust (Table 4), it appears that the Mozambique Belt crust in Kenya, away from the rift proper, has not been significantly modified by the Cenozoic tectonism. Given this conclusion, it seems reasonable to take all of the estimates of Moho depth and Poisson's ratio from Kenya and Tanzania (again away from the rift valleys), and combine them into average values representative of unmodified Mozambique Belt crust. Doing so yields an

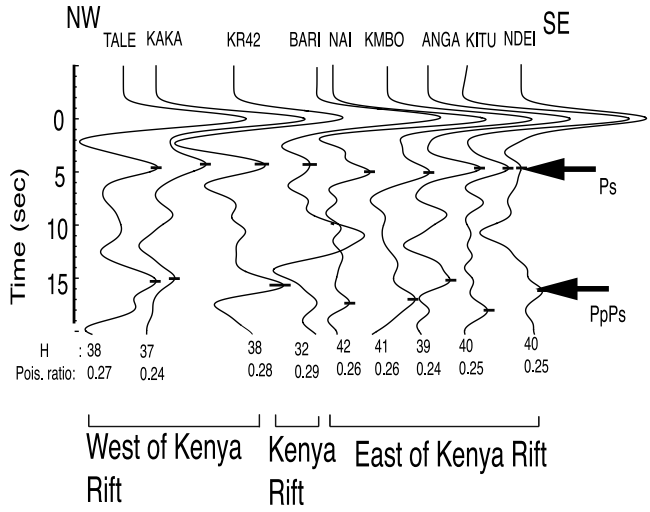

Figure 6. NW-SE profile of receiver functions in Kenya. *H* and Poisson's ratio are from Table 3.

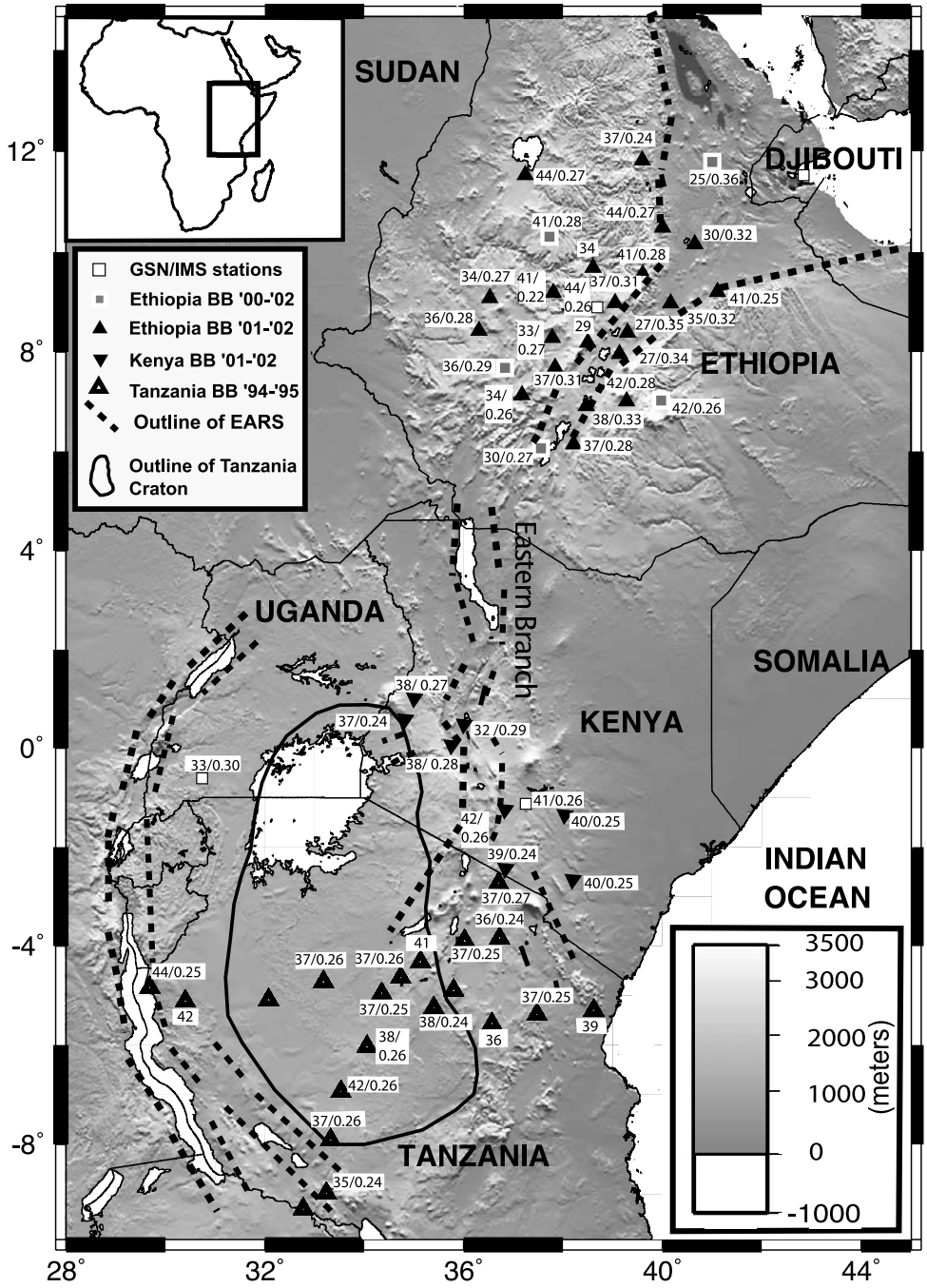

Figure 7. Moho depths and Poisson's ratios (the first and the second numbers next to each station, respectively) obtained in this study and for Tanzania by *Last et al.* [1997].

average Moho depth of 39 ± 2 (SD) km, and an average Poisson's ratio of 0.25 ± 0.01 (SD). The average Poisson's ratio indicates felsic to intermediate composition crust.

[35] There is one station in Kenya within the rift (BARI), and the Moho depth and Poisson's ratio for this station are anomalous with respect to the average Mozambique Belt crust. The crust is thinner by some 7 km (from KRISP refraction profile), and Poisson's ratio is significantly higher (0.29). The high Poisson's ratio indicates that much of the preexisting Mozambique Belt crust has been modified or replaced by mafic intrusions. This finding is consistent with the KRISP refraction results showing high *P* wave velocities throughout most of the crust under the central part of the Kenya Rift [*Mechie et al.*, 1994; *Braile et al.*, 1994].

[36] Moving to the north, Moho depths from 27 to 38 km and Poisson's ratios from 0.27 to 0.35 are found at the six stations within the MER (ARBA, BELA, SELA, NAZA, WASH, WANE, Figure 7). These results are in good agreement with previous refraction studies [*Makris and Ginzburg*, 1987; *Berckhemer et al.*, 1975] (Figure 2). Since the MER is about 70 to 80 km wide, it is necessary to address the effect of dipping Moho structure on the value of the Poisson's ratio, especially for stations near the edge of the rift (e.g., SELA, BELA, WASH), where two different

Table 4. Comparison of Crustal Models Obtained in This Study With Global Averages

Source	Country	Region	Moho Depth, km (±3.0)	Poisson's Ratio (±0.02)
This paper	Ethiopia	Afar Depression	25	0.36
		MER	27–38	0.27–0.35
		eastern Ethiopia Plateau	37–42	0.25–0.28
		western Ethiopia Plateau	34–44	0.24–0.28
	Kenya	Kenya Rift		0.29
		east of Kenya Rift	39–42	0.24–0.28
		west of Kenya Rift	37–38	0.24–0.28
	Uganda	east African Plateau	33	0.30
Christensen and Mooney [1995]	global	Precambrian	41.5 ± 5.8 (SD)	
Rudnick and Fountain [1995]	global	Archean	43.0 ± 6.3(SD)	
		Proterozoic	43.6 ± 4.6(SD)	
Zandt and Ammon [1995]	global	Shields		0.29 ± 0.02(SD)
		Platforms		0.27 ± 0.03(SD)
Durrheim and Mooney [1994]	global	Archean	27–40	
		Proterozoic	40–55	

Moho depths may be sampled by the *P*-to-*S* converted phases (~30 km beneath the MER and ~40 km beneath the plateau). In order to determine if the computed value of σ is biased by *PpPs* phases sampling a deeper crust under the plateau, as opposed to sampling thinner crust under the MER, the effect of a late arriving *PpPs* phase on Poisson's ratio was examined through an analysis of error propagation (Appendix A). As shown in Appendix A, whenever the time difference between the *PpPs* and *Ps* phases increases, Poisson's ratio decreases. A deeper crust tends to reduce the value of Poisson's ratio, and thus the high values of Poisson's ratio found for stations in the MER must be controlled primarily by crustal composition and not variations in crustal thickness.

[37] The variability in Moho depth beneath the MER stations (27 to 38 km) most likely reflects differences locally in the amount of extension and/or thickening from underplating and intrusion. The high Poisson's ratio at all stations except ARBA indicate the presence of mafic crust. Uncertainties associated with individual Poisson's ratio estimates are on the order of 0.02, and thus the values at BELA, WASH and WANE (Table 3) are within the range expected for a mafic crust (about 0.30). Recent results from refraction profiles across and along the MER by the EAGLE group [*Mackenzie et al.*, 2003; *Keller et al.*, 2003] show high *P* wave velocities throughout most of the crust, supporting our finding of a largely mafic crust. The even higher values of Poisson's ratios at SELA and NAZA (0.34 and 0.35, respectively), suggest the possibility of some partial melt within the crust beneath these locations, consistent with the presence of historical magmatic activity within the MER.

[38] The presence of mafic crust beneath many of the MER stations has important implications for understanding strain accommodation within the rift. As noted in section 2.1, *Ebinger and Casey* [2001] have proposed that magmatic segments form the locus of extension in transitional rift settings, such as the MER. In order to change the prerift felsic to intermediate crust (i.e., Mozamibque Belt crust with a Poisson's ration of 0.25) to mafic crust, strain within the MER must be accommodated primarily by mafic intrusions, particularly given only modest amounts of extension (~35% [*Ebinger and Casey*, 2001]). Therefore the mafic composition of the crust we find under the MER stations supports the model of *Ebinger and Casey* [2001].

[39] There is only one station within the Afar depression proper (TEND), and thus it is difficult to make a comparison between crustal structure in the MER and the Afar. Moho depth at station TEND is 25 km, in good agreement with refraction line IV (26 km, Figure 2). Poisson's ratios for the crust beneath station TEND is 0.36, also in good agreement with the results obtained in previous studies, as reviewed earlier. Similar to the MER stations, the high Poisson's ratio is likely caused by a mafic crust plus the presence of partial melt. A similar interpretation for high crustal Possion's ratio for the crust in Afar was given by *Ruegg* [1975], *Searle* [1975], and *Makris and Ginzburg* [1987]. Again, using the results for the Mozambique Belt crust in Kenya and Tanzania as an indication of prerift crustal structure, it is obvious that the felsic to intermediate composition crust that once existed beneath the Afar (and MER) is now almost completely replaced with mafic rock.

[40] Has the Mozambique Belt crust beneath the Ethiopian Plateau been similarly modified by the Cenozoic tectonism? To the east of the MER (Figure 7), Moho depths beneath stations HIRN, HERO, GOBA and CHEF vary between 37 and 42 km, and Poisson's ratios range from 0.25 and 0.28. In comparison to the "average" Mozambique Belt crust, as well as to Precambrian crust elsewhere (Table 4), the crust under the eastern side of the Ethiopian Plateau appears to be largely unmodified by the Cenozoic tectonism. There may be up to 1–2 km of basaltic rock lying at the surface, but this volcanic cover does not appear to add a detectable thickness to the crust or alter the average composition of the crust, at least not within the uncertainties of our estimates of Moho depth and Poisson's ratio (Tables 2 and 3). Certainly, there is little evidence for comparable modification of the crust to what is found beneath the MER.

[41] For the western side of the Ethiopian Plateau, Moho depths are between about 34 and 44 km with a mean of 38 km (Figure 7). The crustal thickness in the northern portion (stations FURI, AAUS, DMRK, BAHI, FICH, BIRH, KARA, DIYA) averages 41 km, and is somewhat different than for the southern portion (stations GUDE, NEKE, DELE, JIMA, TERC, WELK), where the average thickness is 35 km. This difference in crustal thickness has been observed previously in refraction profiles [*Berckhemer et al.*, 1975; *Mackenzie et al.*, 2003]. Interestingly, there does not appear to be a significant change in Poisson's ratio associated with the change in crustal thickness. In the

northern portion of the western plateau, the average Poisson's ratio is 0.27, while for the southern portion the average is 0.28.

[42] The variation in crustal thickness between the northern and southern portions of the Ethiopian Plateau to the west of the MER may reflect both variations in the amount of volcanic rock emplaced on the surface of the crust as well as beneath and within it. *Pik et al.* [2003] show differences in the thickness of the flood basalts of ~1–2 km between the northern and southern portions. This variability in flood basalt thickness could be mirrored at depth by similar differences in crustal underplating. If so, this would provide a reasonable explanation for the difference in crustal thickness observed between the northern and southern portions.

[43] Overall, has crustal structure on the western side of the Ethiopian Plateau been extensively modified by the Cenozoic tectonism? Obviously, there has been at least a few kilometers of basaltic rock added to the crust, similar to the eastern side of the plateau. However, because the average values for Moho depth and Poisson's ratio for the stations on the western side of the plateau are similar to the global average for Precambrian crust (Table 4), and also because they are not significantly different from the average Moho depth and Poisson's ratio for unmodified Mozambique Belt crust in Tanzania and Kenya, we conclude that there has not been extensive alteration of the crust on the western side of the plateau either.

[44] A further comparison can be made between our results and those of similar studies on other continents that have examined variations in Moho depth and Poisson's ratio (or V_p/V_s). In studies from Russia and Australia, a pattern between Moho depth and Poisson's ratio was noticed where Poisson's ratio decreased with increasing crustal thickness for Moho depths of 20 to ~45 km [*Egorkin*, 1998; *Chevrot and van der Hilst*, 2000]. For crust thicker than ~45 km Poisson's ratio increased, and this increase was attributed to mafic underplating [*Egorkin*, 1998; *Chevrot and van der Hilst*, 2000]. Our results show a similar trend of decreasing Poisson's ratio with crustal thickness (crustal thickness varies between 25 and 44 km only). The highest Poisson's ratios are found for the thinnest crust beneath the MER and Afar, and as discussed above reflect the mafic composition of the rifted crust. Lower Poisson's ratios are found for thicker crust under the Ethiopian Plateau and reflect the largely unmodified Proterozoic crust that is beneath the flood basalts.

5. Summary

[45] Crustal structure within Kenya and Ethiopia has been investigated using receiver function analysis of broadband seismic data to determine the extent to which the Proterozoic crust of the Mozambique Belt has been modified by the development of the eastern branch of the East African rift system. Two methods have been used to analyze the receiver functions, the H-κ method, and direct stacks of the waveforms. Crustal thickness to the east of the Kenya rift varies between 39 and 42 km, and Poisson's ratios vary between 0.24 and 0.27. To the west of the Kenya rift, Moho depths vary between 37 and 38 km, and Poisson's ratios vary between 0.24 and 0.27. When these estimates for Moho depth and Poisson's ratio are compared to estimates from a previous study of the Mozambique Belt in Tanzania, as well as to global average values for Proterozoic crust, it appears that the Mozambique Belt crust in Kenya, away from the rift proper, has not been significantly modified by the Cenozoic tectonism.

[46] To the north in Ethiopia, Moho depths vary from 27 to 38 km within the MER, and Poisson's ratios range between 0.27 and 0.35. A crustal thickness of 25 km and a Poisson's ratio of 0.36 were obtained for a single station in the Afar Depression. Beneath the Ethiopian Plateau on either side of the MER, crustal thickness ranges from 33 to 44 km, and Poisson's ratios vary from 0.23 to 0.28. When these estimates of Moho depth and Poisson's ratio are compared to estimates from the Mozambique Belt in Tanzania and Kenya, as well as to global average values for Proterozoic crust, they indicate that the Proterozoic crust away from the Main Ethiopian Rift has also not been modified greatly by the Cenozoic rifting and volcanism. The Cenozoic flood basalts on the Ethiopian Plateau are apparently not thick enough to alter significantly Moho depth beneath the plateau or the bulk composition of the crust. In contrast, the Proterozoic crust beneath the rifted regions (MER and Afar) has been thinned in many places and compositionally altered by the addition of large amounts of mafic rock. This finding supports models suggesting that magmatic segments within the MER, characterized by dike intrusion and Quaternary volcanism, act now as the locus of extension rather than the rift border faults.

Appendix A: Effect on σ From a Step in Crustal Thickness at the Edge of a Rift

[47] Figure A1 illustrates crustal structure at the edge of the Main Ethiopian Rift, where crustal thickness increases from ~30 km to ~40 km. In order to determine the effect on the calculation of the Poisson's ratio of the thicker crust being sampled by the reverberation phases, as opposed to the thinner crust, we begin with the relationships from *Christensen* [1996] and *Zandt et al.* [1995] for Poisson's ratio (σ) and V_p/V_s ratio (κ), respectively:

$$\sigma = \frac{\kappa^2 - 2}{2(\kappa^2 - 1)} \tag{A1}$$

$$\kappa = \sqrt{\left(1 - p^2 V_p^2\right)\left(2\left(\frac{t_{pS} - t_p}{t_{PpPs} - t_{Ps}}\right) + 1\right)^2 + p^2 V_p^2} \tag{A2}$$

where $p = P$ wave ray parameter, t_{Ps}, t_{PpPs} are the arrival times of the *Ps* and *PpPs* phases, respectively, and V_p and V_s are average crustal P wave and S wave velocities, respectively. We consider only the *Ps* and *PpPs* phases because these are the dominant phases in our H-κ stacking and they are the only phases used in the simple stacking method (see sections 3.2 and 3.3). From Figure A1, it can be seen that the arrival time of the *PpPs* phase will be delayed compared to its arrival time if the crust was uniformly 30 km thick. To determine the error introduced by this time delay in the calculation of Poisson's ratio, we apply Taylor series expansion to σ about a value σ_0, which is a Poisson's ratio if the crust is uniformly 30 km thick, and consider only the

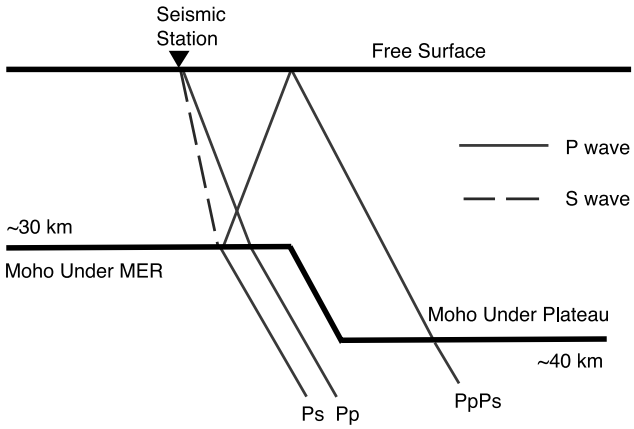

Figure A1. Sketch showing variations in Moho depth near the edge of the MER and rays sampling this structure.

first-order terms in the expansion [e.g., *Bevington and Robinson*, 2003]:

$$\sigma = \sigma_0 + \frac{\partial\sigma}{\partial t_2}\Delta t_2 + \frac{\partial\sigma}{\partial t_1}\Delta t_1 + \frac{\partial\sigma}{\partial p}\Delta p + \frac{\partial\sigma}{\partial V_p}\Delta V_p \qquad \text{(A3)}$$

or

$$\Delta\sigma = \frac{\partial\sigma}{\partial t_2}\Delta t_2 + \frac{\partial\sigma}{\partial t_1}\Delta t_1 + \frac{\partial\sigma}{\partial p}\Delta p + \frac{\partial\sigma}{\partial V_p}\Delta V_p \qquad \text{(A4)}$$

where $t_1 = t_{Ps} - t_P$, $t_2 = t_{PpPs} - t_{Ps}$, and $\Delta\sigma = \sigma - \sigma_0$. For our case (i.e., when we have a step change in the crustal thickness as in Figure A1), t_1 is constant, and we assume, for simplicity, that V_p and p are constant. The right-hand side of equation (A4) and the relationship will then reduce to

$$\Delta\sigma = \frac{d\sigma}{dt_2}\Delta t_2 \qquad \text{(A5)}$$

Applying the chain rule to the derivative and manipulating equations (A1) and (A2) yields

$$\Delta\sigma = -\left[\frac{2\left(1 - p^2V_p^2\right)\left(2\left({}^{t_1}/_{t_2}\right) + 1\right)t_1}{\left(\kappa^2 - 1\right)^2 t_2^2}\right]\Delta t_2 \qquad \text{(A6)}$$

Inspection of equation (A6) reveals that the term in square brackets is positive. Thus the coefficient in front of Δt_2 is negative, and as a result whenever t_2 tends to increase, for example, because of the crustal structure illustrated in Figure A1, σ tends to decrease. Consequently, an offset in the Moho depth near the edge of the MER will tend to decrease σ rather than increase σ.

[48] **Acknowledgments.** We would like to extend our thanks to Laike-Mariam Asfaw and Atalay Ayele, as well as the technical staff of the Geophysical Observatory of Addis Ababa University, for their help with the Ethiopian Broadband Seismic Experiment. We would also like to thank Michel Cara, Sebastian Chevrot, and Isabelle Manighetti for helpful reviews. This research has been funded by the National Science Foundation (grants EAR 993093 and 0003424).

References

Ammon, C. J., G. E. Randall, and G. Zandt (1990), On the nonuniqueness of receiver function inversions, *J. Geophys. Res.*, *95*, 15,303–15,318.

Ayalew, D., P. Barbey, B. Marty, L. Reisberg, G. Yirgu, and R. Pik (2002), Source, genesis, and timing of giant ignimbrite deposits associated with Ethiopian continental flood basalts, *Geochim. Cosmochim. Acta*, *66*, 1429–1448.

Baker, B. H. (1986), Tectonics and volcanism of the southern Kenya Rift valley and its influence on rift sedimentation, in *Sedimentation in the African Rifts*, edited by L. E. Frostick et al., *Geol. Soc. Spec. Publ.*, *25*, 45–57.

Baker, J. A., L. W. Snee, and M. A. Menzies (1996), A brief Oligocene period of flood volcanism in Yemen: Implications for the duration and rate of continental flood volcanism at the Afro-Arabian triple junction, *Earth Planet. Sci. Lett.*, *138*, 39–55.

Bellahsen, N., C. Faccenna, F. Funiciello, J. M. Daniel, and L. Jolivet (2003), Why did Arabia separate from Africa?, *Earth Planet. Sci. Lett.*, *216*, 365–381.

Berckhemer, H., B. Baier, H. Bartlesen, A. Behle, H. Burkhardt, H. Gebrande, J. Markris, H. Menzel, H. Miller, and R. Vees (1975), Deep seismic soundings in the Afar region and on the highland of Ethiopia, in *Afar Depression of Ethiopia*, edited by A. Pilger and A. Rosler, pp. 89–107, E. Schweizerbart, Stuttgart, Germany.

Berhe, S. (1990), Ophiolites in northeast and East Africa: Implications for Proterozoic crustal growth, *J. Geol. Soc. London*, *147*, 41–57.

Berhe, S. M., B. Desta, M. Nicoletti, and M. Teferra (1987), Geology, geochronology and geodynamic implications of the Cenozoic magmatic province in W and SE Ethiopia, *J. Geol. Soc. London*, *144*, 213–226.

Bevington, P. R., and D. K. Robinson (2003), *Data Reduction and Error Analysis for the Physical Sciences*, 3rd ed., pp. 39–41, McGraw-Hill, New York.

Braile, L. W., B. Wang, C. R. Daudt, G. R. Keller, and J. P. Patel (1994), Modeling the 2-D seismic velocity structure across the Kenya Rift, *Tectonophysics*, *236*, 251–269.

Bratt, S. R., and S. C. Solomon (1984), Compressional and shear wave structure of the East Pacific Rise at 11°20′N: Constraints from three-component ocean bottom seismometer data, *J. Geophys. Res.*, *89*, 6095–6110.

Burke, K., and A. M. C. Sengor (1986), Tectonic escape in the evolution of the continental crust, in *Reflection Seismology: The Continental Crust*, *Geodyn. Ser.*, vol. 14, edited by M. Barazangi and L. Brown, pp. 41–53, AGU, Washington, D. C.

Cahen, L., N. J. Snelling, J. Delhal, and J. R. Vail (1984), *The Geochronology and Evolution of Africa*, 512 pp., Oxford Univ. Press, New York.

Chernet, T., W. K. Hart, J. L. Aronson, and R. C. Walter (1998), New age constraints on the timing of volcanism and tectonism in the northern Main Ethiopian Rift–southern Afar transition zone (Ethiopia), *J. Volcanol. Geotherm. Res.*, *80*, 267–280.

Chevrot, S., and R. D. van der Hilst (2000), The Poisson ratio of the Australian crust: Geological and geophysical implications, *Earth Planet. Sci. Lett.*, *183*, 121–132.

Christensen, N. I. (1996), Poisson's ratio and crustal seismology, *J. Geophys. Res.*, *101*, 3139–3156.

Christensen, N. I., and W. D. Mooney (1995), Seismic velocity structure and composition of the continental crust: A global view, *J. Geophys. Res.*, *100*, 9761–9788.

Coulie, E., X. Quidelleur, P. Y. Gillot, V. Courtillot, J. C. Lefevre, and S. Chiesa (2003), Comparative K-Ar and Ar/Ar dating of Ethiopian and Yemenite Oligocene volcanism: Implications for timing and duration of the Ethiopian traps, *Earth Planet. Sci. Lett.*, *206*, 477–492.

Courtillot, V., C. Jaupart, I. Manighetti, P. Tapponnier, and J. Besse (1999), On causal links between flood basalts and continental breakup, *Earth Plant. Sci. Lett.*, *166*, 177–195.

Davidson, A., and D. C. Rex (1980), Age of volcanism and rifting in southwestern Ethiopia, *Nature*, *283*, 657–658.

Dawson, J. B. (1992), Neogene tectonics and volcanicity in the north Tanzania sector of the Gregory rift valley: Contrasts with the Kenya sector, *Tectonophysics*, *204*, 81–92.

Dugda, M. T. (2003), Crustal structure in Ethiopia and Kenya from receiver function analysis, M.S. thesis, 114 pp., Pa. State Univ., University Park.

Durrheim, R. J., and W. D. Mooney (1994), Evolution of the Precambrian lithosphere: Seismological and geochemical constraints, *J. Geophys. Res.*, *99*, 15,359–15,374.

Ebinger, C. J. (1989), Tectonic development of the western branch of the East African rift system, *Geol. Soc. Am. Bull.*, *101*, 885–903.

Ebinger, C. J., and M. Casey (2001), Continental breakup in magmatic provinces: An Ethiopian example, *Geology*, *29*, 527–530.

Ebinger, C. J., T. Yemane, G. WoldeGabriel, J. L. Aronson, and R. C. Walter (1993), Late Eocene-Recent volcanism and faulting in the southern main Ethiopian rift, *J. Geol. Soc. London*, *150*, 99–108.

Ebinger, C., T. Yemane, D. J. Harding, S. Tesfaye, S. Kelly, and D. C. Rex (2000), Rift deflection, migration, and propagation: Linkage of the Ethiopian and eastern rifts, Africa, *Geol. Soc. Am. Bull.*, *112*, 163–176.

Efron, B., and R. Tibshirani (1991), Statistical data analysis in the computer age, *Science*, *253*, 390–395.

Egorkin, A. V. (1998), Velocity structure, composition and discrimination of crustal provinces in the former Soviet Union, *Tectonophysics*, *298*, 395–404.

Foster, A., C. Ebinger, E. Mbede, and D. Rex (1997), Tectonic development of the northern Tanzanian sector of the East African Rift system, *J. Geol. Soc. London*, *154*, 689–700.

Fuchs, K., R. Altherr, B. Muller, and C. Prodehl (Eds.) (1997), Structure and dynamic processes in the lithosphere of the Afro-Arabian Rift system, *Tectonophysics*, *278*, special issue, 352 pp.

George, R., N. Rogers, and S. Kelley (1998), Earliest magmatism in Ethiopia: Evidence for two mantle plumes in one flood basalt province, *Geology*, *26*, 923–926.

Gibson, I. L. (1967), Preliminary account of the volcanic geology of Fantale, Shoa, *Bull.10*, pp. 59–67, Geophys. Obs., Addis Ababa.

Hebert, L., and C. A. Langston (1985), Crustal thickness estimate at AAE (Addis Ababa, Ethiopia) and NAI (Nairobi, Kenya) using teleseismic *P*-wave conversions, *Tectonophysics*, *111*, 299–327.

Hendrie, D. B., N. J. Kusznir, C. K. Morley, and C. J. Ebinger (1994), Cenozoic extension in northern Kenya: A quantitative model of rift basin development in the Turkana region, *Tectonophysics*, *236*, 409–438.

Hofmann, C., V. Courtillot, G. Feraud, P. Rochette, G. Yirgu, E. Ketefo, and R. Pik (1997), Timing of the Ethiopian flood basalt event and implications for plume birth and global change, *Nature*, *389*, 838–841.

Keller, G. R., S. H. Harder, K. Tadesse, P. Maguire, B. M. O'Reilly, K. Mickus, and N. O. Mariita (2003), A preliminary analysis of crustal structure variations along the Ethiopian rift, *Eos Trans. AGU*, *84*(46), Fall Meet. Suppl., Abstract S52J-02.

Kroner, A., R. Greiling, and T. Reischman (1987), Pan-African crustal evolution in the Nubian segment of northeast Africa, in *Proterozoic Lithospheric Evolution*, *Geodyn. Ser.*, vol. 17, edited by A. Kroner, pp. 235–257, AGU, Washington, D. C.

Langston, C. A. (1979), Structure under Mount Rainier, Washington, inferred from teleseismic body waves, *J. Geophys. Res.*, *84*, 4749–4762.

Last, R. J., A. A. Nyblade, C. A. Langston, and T. J. Owens (1997), Crustal structure of the East African plateau from receiver functions and Rayleigh wave phase velocities, *J. Geophys. Res.*, *102*, 24,469–24,483.

Ligorria, J. P., and C. Ammon (1999), Iterative deconvolution and receiver-function estimation, *Bull. Seismol. Soc. Am.*, *89*, 1395–1400.

Mackenzie, G. D., H. Thybo, P. K. H. Maguire, T. Mammo, and M. A. Khan (2003), Crustal velocity structure across the main Ethiopian Rift, *Eos Trans. AGU*, *84*(46), Fall Meet. Suppl., Abstract S52J-03.

Makris, J., and A. Ginzburg (1987), The Afar Depression: Transition between continental rifting and sea floor spreading, *Tectonophysics*, *141*, 199–214.

Manighetti, I., P. Tapponnier, V. Courtillot, S. Gruszow, and P. Y. Gillot (1997), Propagation of rifting along the Arabia-Somalia plate boundary: The gulfs of Aden and Tadjoura, *J. Geophys. Res.*, *102*, 2681–2710.

Mechie, J., G. R. Keller, C. Prodehl, S. J. Gaciri, L. W. Braile, W. D. Mooney, D. J. Gajewski, and K. J. Sandmeier (1994), Crustal structure beneath the Kenya Rift from axial profile data, *Tectonophysics*, *236*, 179–199.

Mechie, J., G. R. Keller, C. Prodehl, M. A. Khan, and S. J. Gaciri (1997), Structure and dynamic processes in the lithosphere of the Afro-Arabian Rift system: A model for the structure, composition and evolution of the Kenya Rift, *Tectonophysics*, *278*, 1–4, 95–119.

Mohr, P. (1983), Ethiopian flood basalt province, *Nature*, *303*, 577–584.

Mohr, P., and B. Zanettin (1988), The Ethiopian flood basalt province, in *Continental Flood Basalts*, edited by J. D. MacDougall, pp. 63–110, Springer, New York.

Morley, C. K., W. A. Wescott, D. M. Stone, R. M. Harper, S. T. Wigger, and F. M. Karanja (1992), Tectonic evolution of the northern Kenyan Rift, *J. Geol. Soc. London*, *149*, 333–348.

Noble, W. P., D. A. Foster, and A. J. W. Gleadow (1997), The post-Pan-African thermal and extensional history of crystalline basement rocks in eastern Tanzania, *Tectonophysics*, *275*, 331–350.

Nyblade, A. A., and R. A. Brazier (2002), Precambrian lithospheric controls on the development of the East African rift system, *Geology*, *30*, 755–758.

Nyblade, A. A., and C. A. Langston (2002), Broadband seismic experiments probe the East African rift, *Eos Trans. AGU*, *83*, 405, 408–409.

Owens, T. J., and G. Zandt (1997), Implications of crustal property variations for models of Tibetan Plateau, *Nature*, *387*, 37–43.

Pik, R., B. Marthy, J. Carignan, and J. Lave (2003), Stability of the upper Nile drainage network (Ethiopia) deduced from (U-Th)/He thermochronometry: Implications for uplift and erosion of the Afar plume dome, *Earth Planet. Sci. Lett.*, *215*, 73–88.

Prodehl, C., G. R. Keller, and M. A. Khan (Eds.) (1994), Crustal and upper mantle structure of the Kenya Rift, *Tectonophysics*, *236*, special issue, 483 pp.

Ritter, J. R. R., and T. Kaspar (1997), A tomography study of the Chyulu Hills, Kenya, *Tectonophysics*, *278*, 149–169.

Rudnick, R. L., and D. M. Fountain (1995), Nature and composition of the continental crust: A lower crustal perspective, *Rev. Geophys.*, *33*, 267–309.

Ruegg, J. C. (1975), Main results about the crustal and upper mantle structure of the Djibouti region (T. F. A. I.), in *Afar Depression of Ethiopia*, edited by A. Pilger and A. Rosler, pp. 120–134, E. Schweizerbart, Stuttgart, Germany.

Searle, R. C. (1975), The dispersion of surface waves across southern Afar, in *Afar Depression of Ethiopia*, edited by A. Pilger and A. Rosler, pp. 113–120, E. Schweizerbart, Stuttgart, Germany.

Searle, R. C., and P. Gouin (1971), An analysis of some local earthquake phases originating near the Afar triple junction, *Bull. Seismol. Soc. Am.*, *61*, 1061–1071.

Shackleton, R. M. (1986), Precambrian collision tectonics in Africa, in *Collision Tectonics*, edited by M. P. Coward and A. C. Reis, *Geol. Soc. Spec. Publ.*, *19*, 329–349.

Tarkov, A. P., and V. V. Vavakin (1982), Poisson's ratio behavior in crystalline rocks: Application to the Study of the Earth's interior, *Phys. Earth Planet. Inter.*, *29*, 24–29.

Vail, J. R. (1985), Pan-African (late Precambrian) tectonic terrains and the reconstruction of the Arabian-Nubian Shield, *Geology*, *13*, 839–849.

Vail, J. R. (1988), Tectonics and evolution of the Proterozoic basement of northeastern Africa, in *The Pan-African Belt of Northeast Africa and adjacent areas*, edited by S. El-Gaby and R. Grieling, pp. 195–226, Friedr. Vieweg, Wiesbaden, Germany.

van der Beek, P., E. Mbede, P. Andriessen, and D. Delvaux (1997), Passive margin uplift around the North Atlantic region and its role in Northern Hemisphere late Cenozoic glaciation: Discussion and reply, *Geology*, *25*, 282–283.

Watanabe, T. (1993), Effects of water and melt on seismic velocities and their application to characterization of seismic reflectors, *Geophys. Res. Lett.*, *20*, 2933–2936.

WoldeGabriel, G., J. L. Aronson, and R. C. Walter (1990), Geology and geochronology, and rift basin development in the central sector of the main Ethiopian rift, *Geol. Soc. Am. Bull.*, *102*, 439–458.

WoldeGabriel, G., R. C. Walter, W. K. Hart, S. A. Mertzman, and J. L. Aronson (1999), Temporal relations and geochemical features of felsic volcanism in the central sector of the main Ethiopian Rift, *Acta Vulcanol.*, *11*, 53–67.

Wolfenden, E., C. Ebinger, G. Yirgu, A. Dieno, and D. Ayalew (2004), Evolution of the northern main Ethiopian Rift: Birth of a triple junction, *Earth Planet. Sci. Lett.*, *224*, 213–228.

Zandt, G., and C. J. Ammon (1995), Poisson's ratio of Earth's crust, *Nature*, *374*, 152–155.

Zandt, G., S. C. Myers, and T. C. Wallace (1995), Crust and mantle structure across the Basin and Range–Colorado Plateau boundary at 37°N latitude and implications for Cenozoic extensional mechanism, *J. Geophys. Res.*, *100*, 10,529–10,548.

Zanettin, B., E. Justin-Visentin, M. Nicoletti, and E. M. Piccirllo (1980), Correlations among Ethiopian volcanic formations with special references to the chronological and stratigraphical problems of the "Trap Series," *Atti Conv. Lincei*, *47*, 231–252.

Zhu, L., and H. Kanamori (2000), Moho depth variation in southern California from teleseismic receiver functions, *J. Geophys. Res.*, *105*, 2969–2980.

C. J. Ammon, Department of Geosciences, Pennsylvania State University, 440 Deike Bldg., University Park, PA 16802, USA.

M. T. Dugda, Department of Geosciences, Pennsylvania State University, 410 Deike Bldg., University Park, PA 16802, USA. (mulugeta@geosc.psu.edu)

J. Julia, Division of Earth and Ocean Sciences, Duke University, 106A Old Chem, Box 90227, Durham, NC 27708, USA.

C. A. Langston, Center for Earthquake Research and Information, University of Memphis, 3876 Central Avenue, Suite 1, Memphis, TN 38152-3050, USA.

A. A. Nyblade, Department of Geosciences, Pennsylvania State University, 447 Deike Bldg., University Park, PA 16802, USA.

S. Simiyu, Kenya Power Generating Company, P.O. Box 1202, Naivasha, Kenya.